JOURNAL OF PROPULSION AND POWER
Vol. 31, No. 4, July–August 2015

Structural Dynamics Optimization of Rotor Systems for a Small-Size Turboprop Engine

Alexander O. Pugachev*
Technische Universität München, 85748 Garching, Germany
and
Alexander V. Sheremetyev,† Viktor V. Tykhomirov,‡ and Oleg I. Shpilenko§
Ivchenko Progress, 69068 Zaporozhye, Ukraine

DOI: 10.2514/1.B35399

This paper presents the results of the rotordynamic analysis and design optimization performed for a turboprop engine-rotor system consisting of a free-power turbine and a gas generator. Predictions of static stresses, natural frequencies, and amplitudes are obtained by the in-house finite-element code. A detailed analysis of the finite-element method model (various beam formulations, three-dimensional axisymmetric model, point masses, and one-dimensional rigid disk elements) is provided. A sizing optimization problem of total shaft mass minimization is considered. Design variables are inner radii and wall thicknesses of shaft sections. Constraints are imposed on static stresses, natural frequencies, and amplitudes of the unbalance response. Changes in design variables are constrained to avoid contacts between the shafts of the twin-spool configuration. An in-house implementation of the sequential quadratic programming method is coupled with hybrid, analytical and numerical, sensitivity analysis. Results of the optimization show that a significant mass reduction in comparison with the baseline configuration can be achieved with all constraints being simultaneously satisfied. The optimal designs, however, must be finalized to meet other requirements not considered during the optimization. The Campbell diagram of the free-power turbine rotor system is significantly affected by the optimization.

Nomenclature

A	=	beam cross-sectional area
a	=	amplitude
$\boldsymbol{C}$	=	damping matrix
c_s	=	shear deformation coefficient
E	=	elasticity modulus
$\boldsymbol{F}$	=	force vector
F_h	=	harmonic force
FT	=	free-power turbine rotor system
$\boldsymbol{G}$	=	gyroscopic matrix
G	=	shear modulus
GG	=	gas generator rotor system
h	=	design variable
I^a	=	beam area moment of inertia
I_d	=	disk diametral moment of inertia
I^p	=	beam polar moment of inertia
J_d	=	disk polar moment of inertia
K_t	=	torsional stiffness coefficient
$\boldsymbol{K}$	=	stiffness matrix
L	=	beam finite-element length
$\boldsymbol{M}$	=	mass matrix
M^b	=	bending moment
M_d^g	=	disk gyroscopic moment
M_t	=	torsional mass coefficient
m_d	=	disk mass
m_{sh}	=	shaft mass
N_A	=	length of the frequency vector for Campbell and harmonic analyses
N_E	=	number of beam finite elements
N_F	=	number of natural frequency constraints
n_{cr}	=	critical speed
p	=	complex eigenvalue
R_{in}	=	shaft section inner radius
R_{out}	=	shaft section outer radius
T	=	torque
T_d	=	shaft torque
u	=	state variable
W_d	=	disk weight force
$\boldsymbol{y}$	=	eigenvector
y_h	=	harmonic response
Δ	=	shaft section wall thickness
κ	=	shear factor
λ	=	natural frequency
μ^m	=	mass per unit length
ν	=	Poisson's ratio
ξ	=	modal damping
ρ	=	density
σ_b	=	bending stress
σ_{eqv}	=	equivalent stress
τ	=	torsional stress
ω	=	rotational speed

I. Introduction

AN IMPORTANT direction in the air-breathing propulsion technology is the development of advanced small-size turboprop engines in the power range below 1000 kW. Delivering the requirements for operational reliability, efficiency, ecological compatibility, and noise is directly connected with the design and analysis of the whole rotor system of a gas-turbine engine. Significant features of advanced turboprop engines are high-speed engine core, high-pressure ratio centrifugal compressor, cooled turbine, and high-speed ratio propeller gearbox. Additionally, all components of the engine have to be as light as possible. Therefore, design of lightweight high-speed shafts must include comprehensive stress and rotordynamic analyses to ensure structural integrity and dynamic stability of rotating parts. Using the mathematical methods of optimization and sensitivity analysis coupled with comprehensive theoretical models of turboprop engine components can help

Received 27 March 2014; revision received 24 October 2014; accepted for publication 14 January 2015; published online 26 March 2015.

*Research Associate, Institute of Energy Systems.
†Head, Strength Department.
‡Principal Engineer, Strength Department.
§Project Engineer, Strength Department.

exploring potential gains of new designs and speed up the design process.

Theoretical and experimental tasks of the structural and dynamic analyses that should be addressed during the design of lightweight structures are related to deriving the following results: static and dynamic stresses including information on low-cycle and high-cycle fatigue; damped bending and torsional natural frequencies, critical speeds; separation margins and critical speed maps; amplitude-frequency characteristics due to the unbalance response, amplification factors; system stability; shaft orbits during diverse time transient excitations; transmitted forces; balancing; bladed disk vibration; rotor–stator interaction.

Finite-element methods are widely used to perform stress and dynamic analysis of rotating structures. However, a careful selection is required of a specific formulation of the finite-element method to model lightweight rotor systems of aeroengines taking into account configuration, soft-mounting, subsystem links, interaction between the rotating components and the casing, etc. [1,2].

Among the basic optimization problems involving the rotordynamic analysis are minimization of shaft weight [3–8] and removal of rotor critical speeds from the operating range [9,10]. The design variables are usually the shaft cross-section properties (inner and outer radii) as well as bearing stiffness and damping coefficients. The interaction between the objective function and multidisciplinary constraints can give rise to various problems of obtaining strictly optimal solutions. However, the practical, industry-related, optimization studies aim, first of all, at finding improved designs, which in some cases is carried out at the expense of reduced mathematical rigor.

Results presented in [3] for the shaft minimization problem with constraints on critical speeds showed that the optimal shaft shapes could depend on the initial (baseline) shape and an applied optimization method. Bearing and disk positions were considered as design variables in [4] to solve the multi-objective problem of minimization of shaft weight and forces transmitted at the bearings. The results also demonstrated dependence on the optimization method.

The linear matrix inequalities approach was adopted in [11] for optimal selection of bearing rotordynamic coefficients to minimize the rotor unbalance response.

Application of the gradient-based optimization methods requires calculation of derivatives for objective functions and constraints with respect to design variables and performance characteristics. For some optimization problems with frequency and amplitude constraints, performing the sensitivity analysis analytically can be a relatively hard problem, and so it can be replaced by the straightforward numerical sensitivity analysis as was done in [7].

Along with the nonlinear programming methods, genetic algorithms were also widely used in the optimization of rotor systems [12–15]. Genetic algorithms have an advantage of being capable of finding the global optimum point; however, they would need considerably larger number of iterations as compared to the gradient-based methods.

The goal of this study is to demonstrate how the mass, static, and rotordynamic properties of an aeroengine twin-spool rotor system can be improved using the design optimization methods. A distinguishing feature of this work is the application of a combined optimization approach to a multiple-shaft system coupled with the static, modal, and harmonic finite-element analyses.

Simultaneous minimization of the mass of a free-power turbine shaft and a gas generator shaft is considered in this work. The constraints are imposed on static and equivalent stresses, natural frequencies, and amplitudes of the unbalance response. Design variables are inner radii and wall thicknesses of shaft sections. The in-house optimization environment based on a sequential quadratic programming technique and developed in [16,17] is extended to the analysis of twin-spool rotor systems. Calculation of derivatives for the objective function and constraints on stresses and amplitudes in respect to design and state variables is performed in the analytical form. Numerical sensitivity analysis is used for the the modal equation. The stress and rotordynamic analyses are performed using an in-house finite-element code. The rotor system of a prototype small-size turboprop engine is used as a baseline design. Configuration of the turboprop engine under consideration is shown in Fig. 1.

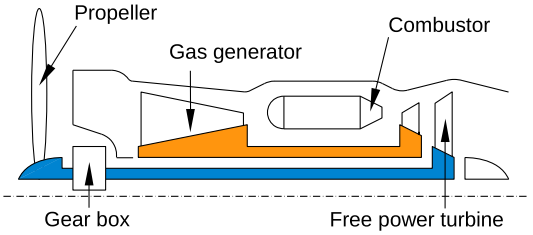

Fig. 1 Configuration of a small-size turboprop engine.

The structure of the paper is as follows. Section II presents rotordynamic modeling based on the Timoshenko beam formulation used in the optimization environment. Section III describes baseline design of the studied twin-spool rotor system and compares results of the rotordynamic analysis obtained with different finite-element models. Section IV describes the optimization problem and briefly presents components of the developed optimization environment. Results of three optimization runs with different limits of design variables are discussed in Sec. V. The final section summarizes the findings presented in the paper.

II. Rotordynamic Modeling of Rotor Systems

The stress and rotordynamic analyses of a rotor system are performed using the finite-element method (FEM) implemented in the in-house code MRACE developed in MATLAB. An FEM formulation is based on a standard two-node circular hollow beam element with 10 degrees of freedom. Axial nodal displacements are not considered. Bernoulli–Euler and Timoshenko beam formulations are available. The shear deformation coefficient in the Timoshenko beam formulation is calculated as follows ([18] p. 215):

$$c_s = \frac{12EI^a}{L^2GA\kappa} \tag{1}$$

where κ is the shear factor, the value of which depends on the cross-sectional shape of a beam ($\kappa = 0.53$ for a thin hollow cylindrical beam).

The equation of motion for the complete rotor system including the gyroscopic effect and damping can be written in matrix form as ([18] p. 219)

$$\boldsymbol{M}\ddot{u} + (\boldsymbol{G} + \boldsymbol{C})\dot{u} + \boldsymbol{K}u = \boldsymbol{F} \tag{2}$$

The effect of torsion is modeled using the torsional stiffness and torsional mass:

$$K_t = \frac{2I^aG}{L}, \qquad M_t = \frac{2\rho I^aL}{3} \tag{3}$$

The local finite-element matrices for the Timoshenko beam formulation are summarized in the Appendix. The schematic of the beam element is also shown in the Appendix.

Bearings are modeled as anisotropic spring–damper elements. Disks are modeled as point masses (zero-dimensional, or 0-D, disk) or two-node one-dimensional (1-D) rigid elements (1-D disk) with specified inertial characteristics. In the latter case, the mass matrix of the disk element and the mass and stiffness matrices of the corresponding beam element as well as the derivatives needed for the optimization method are transformed accordingly to the kinematic coupling between two nodes of the rigid element. The local finite-element matrices of the disk element and the transformation matrix are summarized in the Appendix [Eq. (A8)]. Transformation of the beam element matrices is performed by analogy (see [18] pp. 220–221).

A. Static Analysis

The static analysis is used to obtain static stresses in the shaft sections by solving the following equation:

$$\boldsymbol{K}u = \boldsymbol{F} \tag{4}$$

The static force vector $\boldsymbol{F}$ includes the disk weight force W_d, the disk gyroscopic moment M_d^g, and the shaft torque T_d.

Based on the conventional assumption about the shaft stress condition, the bending stress σ_b, torsional stress τ, and equivalent stress σ_{eqv} are calculated as

$$\sigma_b = \frac{M^b R_{\text{out}}}{I^a}, \qquad \tau = \frac{TR_{\text{out}}}{2I^a}, \qquad \sigma_{\text{eqv}} = \sqrt{(\sigma_b)^2 + 3\tau^2} \tag{5}$$

The element bending moment M^b and torque T are obtained from the local element force vector $\boldsymbol{F}^e$:

$$M^b = 0.25L(\boldsymbol{F}_1^e + \boldsymbol{F}_2^e + \boldsymbol{F}_6^e + \boldsymbol{F}_7^e) + 0.5(\boldsymbol{F}_3^e + \boldsymbol{F}_4^e + \boldsymbol{F}_8^e + \boldsymbol{F}_9^e)$$
$$T = 0.5(\boldsymbol{F}_5^e + \boldsymbol{F}_{10}^e) \tag{6}$$

where $\boldsymbol{F}^e$ is the local force vector calculated for each beam element by multiplying the local stiffness matrix $\boldsymbol{k}^e$ by the corresponding state variables u^e.

The static analysis is performed for the operating speed only (i.e., at constant load). The dynamic stresses occurring during the passage through the critical speeds are not taken into account in this analysis. The information of the equivalent stresses can be used to make a preliminary assessment on the high-cycle fatigue. This, however, is beyond the scope of this work.

B. Modal Analysis

The state equation for the modal analysis is a system of motion equations describing the free vibrations:

$$p^2\boldsymbol{M}y + p(\boldsymbol{G} + \boldsymbol{C})y + \boldsymbol{K}y = 0 \tag{7}$$

where $p = \xi + \sqrt{-1}\lambda$ is the complex eigenvalue. The imaginary parts of complex eigenvalues are natural frequencies, whereas the real parts of eigenvalues are modal damping factors, which contain the information on the stability of the corresponding mode. The negative real part indicates a stable mode. The modal equation is used to calculate the natural frequencies and forms of rigid-body, bending, and torsional modes as well as critical speeds and critical speed maps. The Campbell diagram is obtained by performing the modal analysis for a range of rotational speeds and is used to predict the critical speeds of the rotor system.

Equation (7) is a quadratic eigenvalue problem due to the gyroscopic and damping effects. The quadratic eigenvalue problem can be solved directly or converted to the generalized linear eigenvalue problem consisting of the generalized mass and stiffness matrices twice as large as matrices of the original quadratic eigenvalue problem. The transformation from the second-order problem to the first-order problem can be performed in several ways (see [19]).

C. Harmonic Analysis

Taking into account only harmonic excitation forces (e.g., mass unbalance force), the equations of motion can be reduced to the following harmonic equation:

$$(-\omega^2\boldsymbol{M} + i\omega\boldsymbol{G} + i\boldsymbol{C} + \boldsymbol{K})y_h = F_h \tag{8}$$

Harmonic analysis is used to predict the amplitude–frequency curve for each node of the finite-element model of the rotor system. The unbalance force is represented in a harmonic form $F_h e^{i\omega t}$ and applied to a node where the disk is located. The harmonic equation is solved for a range of rotational speeds ω_i up to the nominal operating speed ω_0.

III. Baseline Design of a Turboprop Rotor System

The baseline design of a prototype turboprop engine-rotor system is shown in Fig. 2. It is a two-shaft engine with straight-flow configuration (see Fig. 1). The gas generator consists of a single-stage centrifugal compressor and a single-stage turbine and is supported by two rolling element bearings. The propeller is driven by the single-stage free-power turbine tailed through a gearbox. The free-power turbine rotor is supported by two rolling element bearings. In the presented analysis, the free-power turbine rotor system also includes the first stage of the gearbox for the accurate prediction of critical speeds. The shaft of the gearbox is supported by two rolling element bearings. The gas generator and free-power turbine shafts are not interconnected (no intershaft bearing). The average inner radius of the gas generator shaft is 16 mm. The smallest gap between two spools is 1.5 mm. The lengths of the free-power turbine rotor and gas generator systems are about 592 and 319 mm, respectively.

The beam model of the studied rotor system is also shown in Fig. 2. The six bearings are shown as vertical segments. The gray boxes

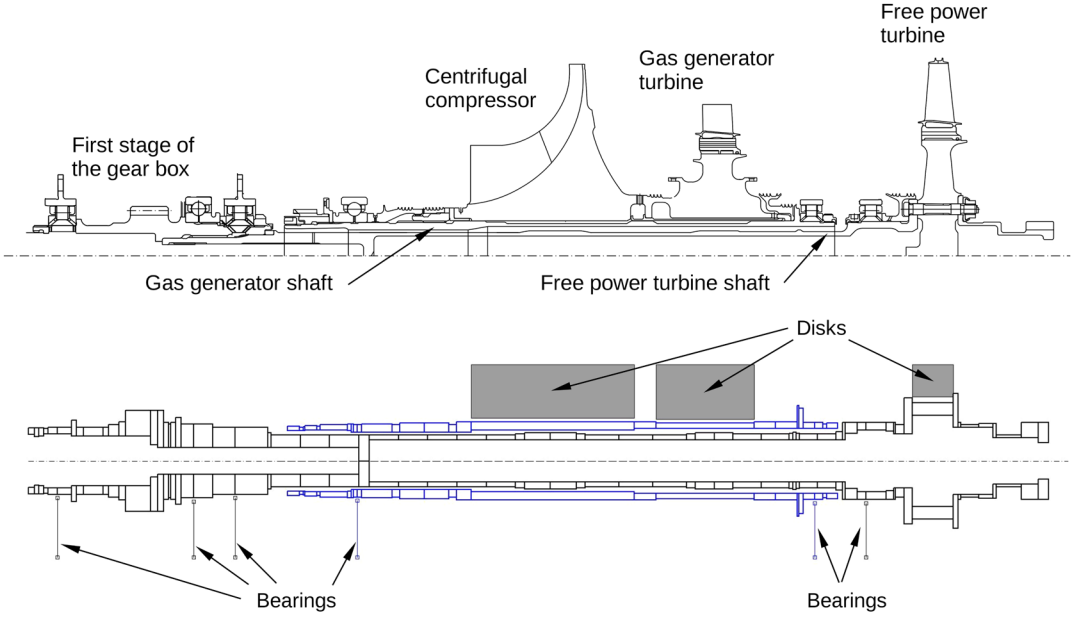

Fig. 2 Configuration (top) and beam-based model (bottom) of the baseline turboprop engine-rotor system.

Table 1 Mass-inertial properties of disks and loads for the turboprop engine-rotor system

		Gas generator	
Parameter	Free-power turbine	Compressor	Turbine
m_d, kg	3.64	3.94	3.23
J_d, kg · m^2	0.0143	0.01182	0.00815
T_d, N · m	87.04	70.14	70.14
M_d^g, N · m	126.79	137.15	94.57
W_d, N	142.69	155.44	126.62
ω_0, rpm	42,356	55,430	55,430

represent rigid elements where the compressor and turbine disks are located.

Table 1 summarizes loads and mass-inertial properties of the disks. The magnitude of disk diametral moment of inertia I_d is assumed to be equal to one-half of its polar moment of inertia. The magnitude of the disk weight force is calculated using the safety factor of 1.5. The material properties for both shafts are $\rho = 7840$ kg/m^3, $E = 1.95 \times 10^{11}$ Pa, $\nu = 0.3$.

The rear roller bearing located near the free-power turbine wheel has the stiffness coefficient of 4.3×10^6 N/m and is equipped with a squeeze film damper. Based on the design experience, the stiffness coefficients of the gearbox bearings can be assumed to be equal when performing rotordynamic analysis of the free-power turbine system. The bearings of the gearbox shaft have the stiffness coefficients of 50×10^6 N/m. The gas generator shaft is supported by two bearings with stiffness coefficients of 6×10^6 and 67×10^6 N/m, respectively. The bearings are modeled as isotropic supports. The bearing stiffness values were obtained in the previous work using a three-dimensional finite-element analysis. The predicted stiffness coefficients were confirmed with the available experimental data for prototype engines of similar size.

A. Results Obtained with the Beam-Based Model

Table 2 summarizes the results obtained with the beam-based models for the baseline designs of free-power turbine and gas generator rotor systems. The torsional natural frequencies are not presented in this work. In the harmonic analysis, the excitation forces are applied at the disk locations. Indicative values are used for the magnitude of the unbalance force to demonstrate typical harmonic response of the studied rotor systems. Dissipative effects in the system apart of the damping provided by the squeeze film damper are taken into account by a common assumption of the shaft element damping matrix being proportional to the shaft element stiffness matrix. A value of 1% is used for the constant structural damping ratio (ratio between actual damping and critical damping ([20] p. 6)), which is an adequate estimation for lightly damped structures.

For comparison, the results obtained using ANSYS Mechanical software package are also shown in Table 2. A high-fidelity beam-based model RACE was developed in ANSYS Mechanical to perform static, modal, Campbell, and harmonic analyses using the beam finite element BEAM189. The bearings are modeled with the finite element COMBI214. The disks are modeled with the finite element MASS21. The rigid elements are modeled with the command CERIG.

The beam model of the free-power turbine rotor including gearbox shaft consists of 56 cylindrical sections (see Fig. 2). All formulations (0-D disk vs 1-D disk, Timoshenko vs Bernoulli–Euler, in-house code vs ANSYS) provide consistent results with rather small discrepancies. This is due to the relatively thin turbine disk.

The beam-based model of the gas generator consists of 25 cylindrical sections. In contrast to the free-power turbine, the gas generator has a rather wide compressor and turbine disks. In this case, application of the Bernoulli–Euler formulation and 0-D disk formulation would lead to inadequate predictions. Therefore, the results for the gas generator are presented only for the Timoshenko beam element and rigid disk sections. The predictions of maximal torsional and equivalent stresses are in good agreement. The in-house code predicts higher bending stresses. The discrepancies in the first four natural frequencies and critical speeds are small. Regarding the harmonic response, the values of maximal disk amplitudes are higher in the in-house code. This could also be due to the different vectors of excitation frequency used in the codes. Although the in-house code uses nonuniform distribution of the excitation frequency (with more dense distribution in the regions of natural frequencies), the ANSYS model uses a uniformly distributed excitation frequency vector. The size of the excitation frequency vector used in the Campbell and harmonic analyses is 120.

Figure 3 (left) shows the Campbell diagram for the free-power turbine (FT) and gas generator (GG) rotor systems. Both rotor systems have three critical speeds. All modes are stable. The critical speeds of the free-power turbine are located in the low rotational speed range. The third critical speed of the gas generator lies in the upper half of the rotational speed range. For both FT and GG rotor systems, the first two critical speeds are located close together.

Figure 3 (right) shows the harmonic response functions for the free-power turbine and gas generator rotor systems. Results are shown for the maximum amplitudes of the shaft nodes at every calculated frequency and amplitudes at disk locations. Each function has one peak that coincides with the location of the corresponding first critical speed. For the gas generator rotor system, the harmonic responses of the compressor and turbine disks are very similar, with the compressor showing larger amplitudes. Results of the calculation of separation margins and amplification factors for the baseline FT rotor system presented in [21] demonstrated sufficient stability margin.

Table 2 Results obtained with the beam-based models for the baseline configuration

		Free-power turbine						Gas generator	
		Timoshenko		Bernoulli–Euler		ANSYS		Timoshenko	ANSYS
Parameter		0-D disk	1-D disk	0-D disk	1-D disk	0-D disk	1-D disk	1-D disk	1-D disk
m_{sh}, kg		2.324	— —	— —	— —	2.324	— —	1.037	1.037
σ_b^{max}, MPa		90.33	89.75	87.01	87.56	88.88	— —	32.43	16.48
τ^{max}, MPa		40.27	— —	40.27	— —	40.36	— —	24.23	24.28
σ_{eqv}^{max}, MPa		106.55	106.06	103.75	104.25	105.39	— —	41.96	42.05
λ, rpm	1	4,093	3,431	4,145	3,873	3,993	4,148	12,287	12,287
	2	8,899	9,303	8,915	9,629	8,705	8,996	17,472	17,658
	3	12,230	11,668	12,407	11,313	12,573	12,089	38,964	40,503
	4	48,538	52,017	49,914	54,668	47,801	48,958	69,872	68,506
	5	59,973	59,833	62,346	61,857	60,051	60,228	113,010	139,787
	6	85,566	96,295	86,590	98,598	85,326	85,534	— —	— —
n_{cr}, rpm	1	6,960	7,003	6,968	7,753	6,698	7,094	14,397	14,447
	2	7,899	8,287	7,901	8,932	7,605	8,046	15,863	15,973
	3	15,929	14,924	16,157	14,389	16,370	15,728	41,404	42,522
a_d^{max}, mm		0.009	0.008	0.009	0.008	0.010	0.009	Compressor/turbine 0.013/0.008	Compressor/turbine 0.008/0.004

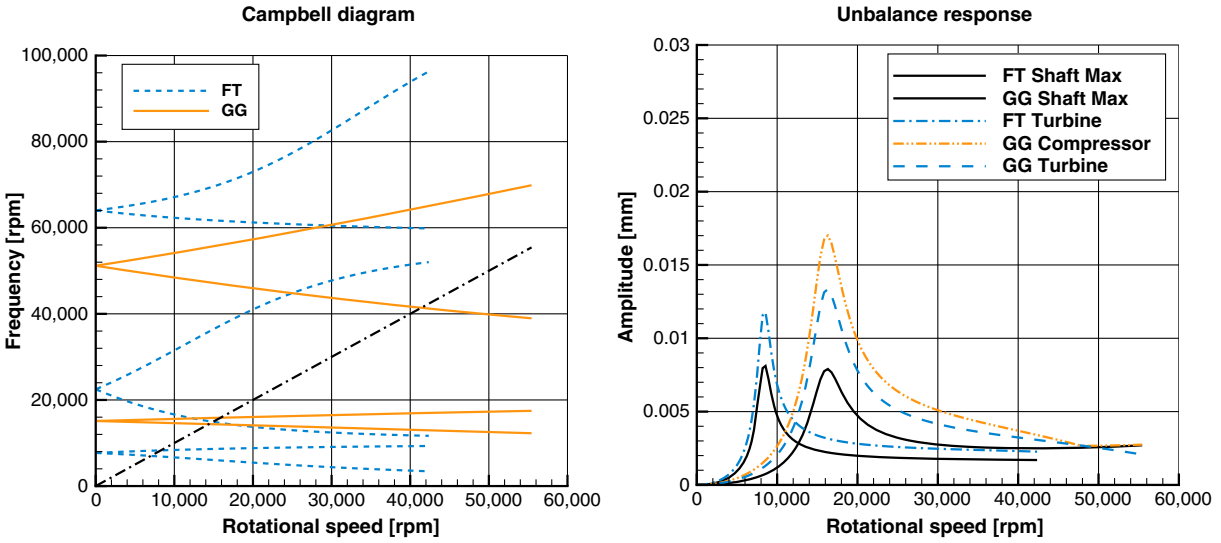

Fig. 3 Results for the baseline design: Campbell diagrams (left) and harmonic response functions (maximal amplitudes and disk amplitudes, right).

B. Verification with Three-Dimensional Axisymmetric Model

The data obtained with the beam-based models are compared with the results of three-dimensional modeling implemented in ANSYS Mechanical [22]. The shaft and disk sections are modeled with a three-dimensional (3-D) axisymmetric solid finite element SOLID272. The sections are first meshed with two-dimensional elements. Then, additional nodes for the axisymmetric elements are generated with the command NAXIS.

The original geometry of the free-power turbine and gas generator is not axisymmetric. The compressor and high-pressure turbine and low-pressure turbine disks have cyclically symmetric geometry. However, rotating structures must be axisymmetric about the rotation axis to perform modal analysis in the stationary reference frame in ANSYS Mechanical [22]. Therefore, the disks must be represented as equivalent cylindrical segments. The density and outer radius of the equivalent disk sections are adjusted to match the mass and moment of inertia of the original compressor and turbine wheels. The following auxiliary optimization problem is considered:

$$\begin{aligned} &\text{Minimize } f = |m_d - m^{\text{eqv}}(\rho^{\text{eqv}}, R_{\text{out}}^{\text{eqv}})| \\ &\text{with constraints } J_d = J^{\text{eqv}}(\rho^{\text{eqv}}, R_{\text{out}}^{\text{eqv}}) \\ &R_{\text{out}}^{\text{eqv}} > R_{\text{in}} \end{aligned} \tag{9}$$

The objective is to minimize the absolute difference between the masses of the real disk m_d and equivalent cylindrical segment m^{eqv}. An equality constraint is imposed on the moment of inertia J^{eqv}. Additional inequality is used to constrain the value of the outer radius of the equivalent cylindrical segment. The axial width and inner radius of the equivalent disk segment are estimated from the original geometry.

The resulting material density values are 8180.52, 2559.82, and 4217.78 kg/m^3 for the equivalent segments representing the free-power turbine, compressor, and high-pressure turbine, respectively. The resulting outer radius values in are 83.32, 74.78, and 68.28 mm for the free-power turbine, compressor, and high-pressure turbine, respectively. As expected, the density and outer radius for the equivalent disk segments take on smaller values than in the real configuration.

Figure 4 shows the three-dimensional models used for the studied rotor systems. Table 3 compares the results of the modal and Campbell analyses performed with the ANSYS beam-based model and ANSYS 3-D model. The lower frequencies calculated with two models are in good agreement for both FT and GG rotor systems. At higher frequencies, the 3-D model tends to predict smaller natural frequencies than the beam-based model. For the calculation of the Campbell diagram, the 3-D model requires considerably more computational time and memory.

IV. Optimization Problem and Environment

A shaft mass minimization problem is considered in this work. The objective function is the total mass of the free-power turbine and gas generator shafts calculated as the sum of masses of each finite element:

$$f = m_{\text{sh}}^{\text{FT}} + m_{\text{sh}}^{\text{GG}}, \qquad m_{\text{sh}} = \rho\pi \sum_{i=1}^{N_E} L_i \Delta_i (2R_{\text{in},i} + \Delta_i) \tag{10}$$

The section inner radius R_{in} and the section wall thickness Δ are selected as design variables h (i.e., there are two design variables per finite element).

The constraint set is defined for each shaft separately. The design variables are constrained by the $4N_E$ simple bounds. Additional $2(N_E - 1)$ constraints are defined to avoid gaps between neighboring shaft elements (δ_o is the predefined magnitude of the overlap):

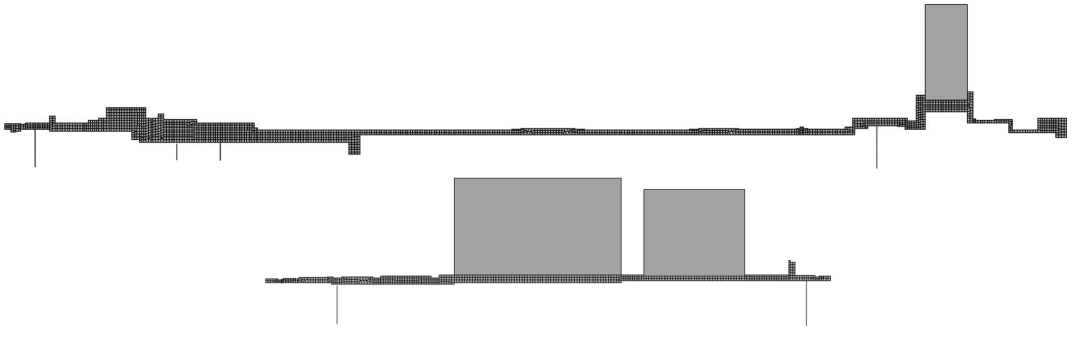

Fig. 4 Three-dimensional models of the free-power turbine (top) and gas generator (bottom).

Table 3 Results obtained with the beam-based and 3-D models for the baseline configuration

		Free-power turbine		Gas generator	
Parameter		Beam	3-D	Beam	3-D
λ, rpm	1	4,148	4,609	12,287	12,226
	2	8,996	9,134	17,658	17,364
	3	12,089	11,623	40,503	36,718
	4	48,958	46,640	68,506	60,933
	5	60,228	54,994	139,787	105,656
	6	85,534	79,083	— —	— —
n_{cr}, rpm	1	7,094	7,387	14,447	14,327
	2	8,046	8,563	15,973	15,767
	3	15,728	15,405	42,522	39,001

$$R_{\text{in},i+1} \le R_{\text{out},i} - \delta_o, \qquad i = 1 \ldots N_E - 1$$
$$R_{\text{out},i+1} \ge R_{\text{in},i} + \delta_o, \qquad i = 1 \ldots N_E - 1 \tag{11}$$

Allowable torsional and equivalent stresses are constrained by upper bounds $\tau^{\max}$ and $\sigma_{\text{eqv}}^{\max}$ ($2N_E$ constraints).

Natural frequencies of rigid-body and bending modes are constrained by the side constraints. The absolute difference between the natural frequencies and operating speed must be greater than or equal to the prescribed value ω_a:

$$|\omega_0 - \lambda_i| \ge \omega_a, \qquad i = 1 \ldots N_F \tag{12}$$

Allowable amplitudes for a predefined location (e.g., location of disks) are constrained by the maximal value $a^{\max}$ ($N_A = 120$ constraints).

Gaps between individual shafts of the twin-spool configurations are constrained with the additional expressions:

$$\delta_{\min} \le R_{\text{in}}^{\text{GG}} - R_{\text{out}}^{\text{FT}} \le \delta_{\max} \tag{13}$$

The latter expressions need an assembly matching vector to define relative positions of the beam elements of the free-power turbine and gas generator. The assembly matching vector is generated automatically during the preprocessing.

Additional equality constraints can be defined to preserve original geometry of the baseline design for particular shaft sections (e.g., the gearbox shaft, etc.).

Other possible design variables (such as axial length of the shafts, bearing span distances, disk locations, etc.) that could alter significantly the rotordynamic behavior are not considered. The optimization presented in this work is formulated to maintain general layout of the engine and is concerned mainly with shaft mass minimization and radial space availability.

A. Optimization Method

The optimization problem defined previously is a nonlinear programming problem, which is solved using the sequential quadratic programming (SQP) technique. A general SQP algorithm consists of three global steps: approximating the Hessian matrix of the Lagrangian function, solving the quadratic programming subproblem, and calculating the step length [23,24]. The Hessian matrix is calculated with the standard Broydon-Fletcher-Goldfarb-Shanno (BFGS) update formula. The step size is obtained through a one-dimensional minimization of the exact penalty function. Details on the optimization method and the in-house optimization environment OMRACE developed in MATLAB can be found in [17].

B. Sensitivity Analysis

The purpose of the sensitivity analysis is to find the effect of changes in the design variables on the objective function and constraints (i.e., the effect of changes in the parameters of the rotor system on its performance). The sensitivity analysis can be performed analytically or numerically by using the finite-difference method. The advantage of the numerical sensitivity analysis is its simplicity. It can be applied straightforward but would take more computational time in comparison with the analytical sensitivity analysis. There are well-developed approaches to perform the sensitivity analysis in analytical form for standard problems of structural mechanics (see [25]). However, the fact that the rotordynamic problems have skew-symmetric gyroscopic matrix complicates the sensitivity analysis of the modal equation.

For the considered optimization problem, sensitivity analysis starts with a linear approximation of variation of the objective function and constraints, which are functions of design variables h and state variables u, λ (natural frequencies), and y_h (displacements). Therefore, sensitivity analysis must be performed for the static, modal, and harmonic equations.

The sensitivity analysis of the static and harmonic equations is performed using the adjoint method [17]. The derivatives of stresses with respect to state and design variables, as well the derivatives of the local finite-element matrices of Timoshenko beam formulation, are obtained directly in the analytical form.

The modal equation represents the main difficulty for the sensitivity analysis. The skew-symmetric gyroscopic matrix makes the generalized eigenvalue problem nonsymmetric, resulting in violation of the assumption necessary for the standard sensitivity analysis of linear eigenvalue problems. Other difficulties are connected with multiple eigenvalues and normalization of complex eigenvectors. There are also methods of calculation of derivatives for the quadratic eigenvalue equations [26] that, however, can face similar technical difficulties.

Applications of analytical methods to compute sensitivity coefficients for the modal equation in the previous works [16,17] were not based upon a strict formalism, yet feasible designs of rotor systems with improved characteristics were obtained using the gradient projection method and sequential quadratic programming.

In this work, sensitivity analysis of the modal equation is performed numerically. The easiest way to find the variation of a performance characteristic is to apply the finite-difference method. The derivatives of interest are calculated numerically using the following central difference formula:

$$\frac{\mathrm{d}\varphi}{\mathrm{d}h_j} \approx \frac{\varphi(h_j + \Delta h) - \varphi(h_j - \Delta h)}{2\Delta h} \tag{14}$$

where φ is either objective function or constraint. The numerical sensitivity analysis is implemented as an extension of the in-house code OMRACE.

V. Results of the Optimization

The extended optimization environment OMRACE is applied to the optimization of the turboprop twin-spool system. The baseline configuration is shown in Fig. 2. Constraints for stresses, natural frequencies, and amplitudes are summarized in Table 4. The frequency margin of 10,000 rpm corresponds to roughly 20% of the operating speeds of two spools. Because the weight of the disks is not changed during the optimization, the unbalance force is kept constant in all optimization runs presented later.

Rather than using the baseline configuration as the initial design, two shafts with a constant cross section are defined as a starting point of the optimization. The following initial values are used for the

Table 4 Parameters for the optimization

Parameter	Value
Allowable torsional stress	245.25 MPa
Allowable equivalent stress	392.40 MPa
Allowable natural frequencies	$\lvert\lambda - \omega_0\rvert \ge 10000$ rpm
Allowable amplitude	0.1 mm

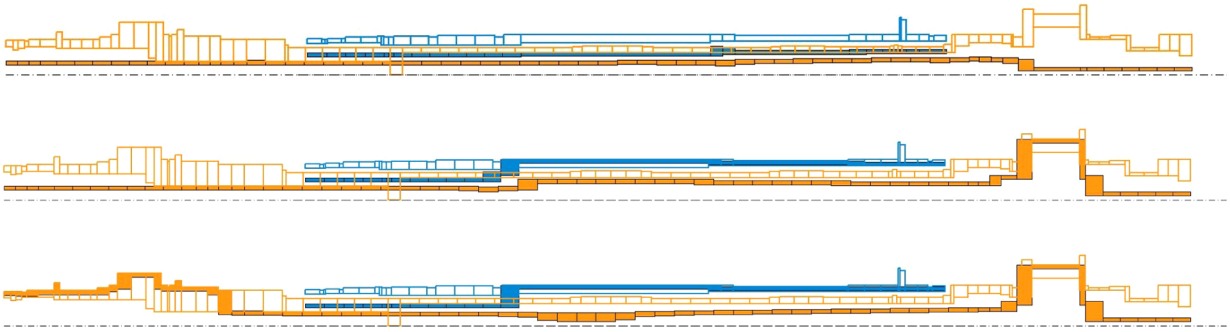

Fig. 5 Optimized shapes of the free-power turbine and gas generator shafts obtained in runs A (top), B (middle), and C (bottom).

design variables: $R_{in} = 3$ mm and $\Delta = 17$ mm for the free-power turbine; $R_{in} = 27$ mm and $\Delta = 10$ mm for the gas generator. The total mass of the oversized initial design is 10.73 kg.

Results of three optimization runs are presented in this work. In optimization run A, general bounds are specified on the design variables. Because cross sections of all shaft sections are free to change within those bounds, this would require necessary adjustments to the geometry of the disks (disk bore diameters) in the optimized configuration. Optimization run B additionally constrains the outer radius of the shaft sections where the disks are mounted. The value of the section outer radius must be the same as in the baseline configuration. In this case, the disks can be directly used with the optimized shape without any modifications. In optimization run C, additional equality constraints on the outer radius of the gearbox shaft are considered to obtain more practical optimal designs.

The optimal shapes of spools obtained in three optimization runs are shown in Fig. 5. Filled-in areas correspond to the optimized shapes, whereas the thin outline shows the baseline design taken from a prototype engine. Optimization runs A, B, and C need 24, 27, and 18 iterations, respectively, to converge. Comparison of the performance of the optimized configurations is summarized in Table 5. Performed on a Linux-based desktop computer, a typical optimization run takes up to several tens of hours. The great deal of computing time per iteration is spent on solving the harmonic equation and performing the sensitivity analysis.

The optimum design A had a total mass of 0.725 kg, which is a considerable reduction as compared to the baseline design with a total mass of 3.361 kg. A visible material removal occurs in the region of the gearbox shaft of the free-power turbine. Another reason for the mass reduction is the notably smaller cross-sectional area of the shafts. The average outer radius of the gas generator shaft is about 12 mm in the optimized design A. Both shafts of the optimized configuration A have nearly the same mass. Because of the additional constraints imposed on the disk bore diameters, the optimal design B has slightly higher mass than the optimal design A, but still the shaft mass reduction in the optimization run B is more than 60% as compared to the baseline design. The optimal design C with additional constraints imposed on the gearbox shaft has total mass less than 50% of the baseline design mass. Although the FT mass is increased due to the additional constraints as compared to the optimal design B, the mass of the GG shaft is slightly reduced in the optimal configuration C. The influence of the gearbox shaft on the free-power turbine rotor system is evident when comparing the optimal shapes obtained in the runs B and C. The shapes of the free-power turbine shaft are quite different.

Table 6 Critical speeds calculated with the ANSYS beam-based and 3-D models

	Critical speed n_{cr}, rpm				
Optimal design C	1	2	3	4	5
FT, beam	3,674	7,220	11,120	30,313	32,512
FT, 3-D	3,976	7,910	11,466	28,898	30,695
GG, beam	13,428	15,021	41,082	— —	— —
GG, 3-D	13,238	15,362	36,506	— —	— —

Table 5 Comparison of the optimization results

		Optimal design A		Optimal design B		Optimal design C	
Parameter		FT	GG	FT	GG	FT	GG
m_{tot}, kg			0.725		1.290		1.546
m_{sh}, kg		0.3706	0.3544	0.7178	0.5723	0.9774	0.5681
σ_b^{max}, MPa		338.29	134.28	338.29	64.52	338.29	76.24
τ^{max}, MPa		226.55	60.77	226.55	61.62	226.08	61.21
σ_{eqv}^{max}, MPa		392.40	165.76	392.40	124.72	392.40	130.58
λ, rpm	1	583	10,425	748	11,368	556	10,908
	2	9,410	14,683	9,279	16,706	9,290	16,319
	3	10,239	27,124	10,099	36,787	10,094	36,267
	4	29,227	65,430	31,197	73,448	31,248	73,377
	5	30,164	66,310	32,356	102,150	32,356	102,596
	6	96,295	— —	75,234	— —	84,521	— —
n_{cr}, rpm	1	3,544	12,413	4,054	13,618	3,521	13,196
	2	7,522	13,421	7,761	15,048	7,555	14,607
	3	11,093	31,926	11,070	39,875	10,991	39,435
	4	28,639	— —	30,696	— —	30,764	— —
	5	30,290	— —	32,480	— —	32,473	— —
a^{max}, mm		0.026	0.024	0.019	0.019	0.021	0.021
a_d^{max}, mm		— —	Compressor/turbine	— —	Compressor/turbine	— —	Compressor/turbine
		0.013	0.024/0.016	0.011	0.018/0.011	0.011	0.020/0.012

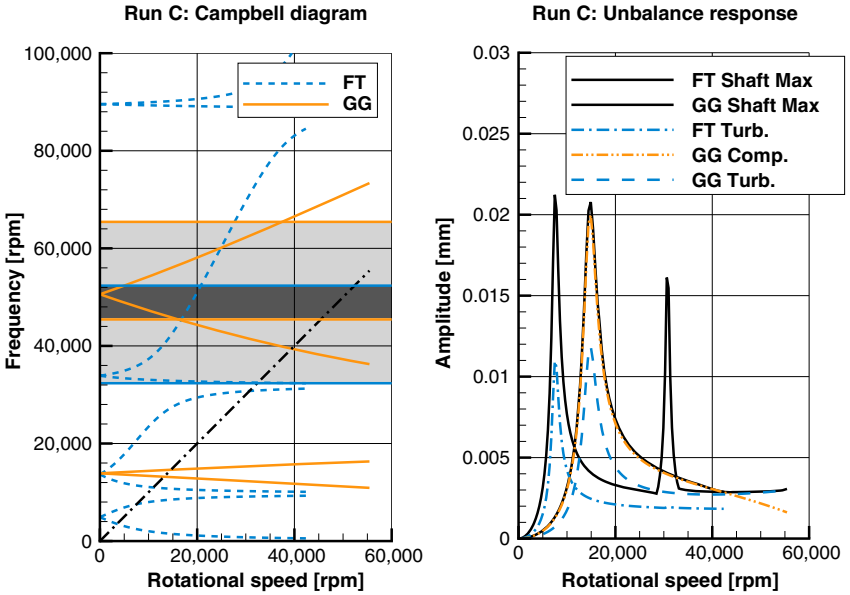

Fig. 6 Results for the optimized shape C: Campbell diagram (left) and harmonic response curves (right).

As expected, the maximal stress levels are increased considerably for all optimal designs (see Table 5). The optimized free-power turbine shaft has active constraints on the equivalent stress. All the natural frequencies are outside of the specified range. Considerable changes for some natural frequencies can be observed. Amplitude constraints are inactive for the final solutions obtained in all optimization runs.

The critical speeds are not constrained during the optimization. Table 5 demonstrates that the values of critical speeds calculated in the postprocessing are changed significantly as compared to the baseline design. The optimized shape of the free-power turbine reveals five critical speeds, which is two critical speeds more than in the baseline configuration. The Campbell diagram for the optimized shape C is shown in Fig. 6 (left). All modes are stable. The shaded areas in the Campbell diagram define the keep-out regions for natural frequencies of two spools. All critical speeds for the free-power turbine and gas generator are also well below the specified frequency range. The harmonic response curve for the optimized shape C is shown in Fig. 6 (right). The free-power turbine rotor system reveals a second peak in the function of maximal amplitudes. Similar Campbell diagrams and harmonic response curves are obtained for the optimal designs A and B. The absolute differences in natural frequencies and critical speeds between the optimal designs A, B, and C are relatively small.

During the postprocessing, the optimized configurations are also analyzed, applying the three-dimensional axisymmetric model described previously. For the optimal design A, new values of the parameters are used for the equivalent cylindrical segments due to the altered bore diameters of the disks. The predicted critical speeds for the optimal design C are shown in Table 6. The agreement between the results is satisfactory. Similar results are obtained for the optimal designs A and B.

Obviously, the optimized shaft shapes must be finalized by designing various technological constituents (labyrinths, heat shields, etc.) and taking into account all manufacturing and gas flow path requirements. The manufacturing requirements can be naturally included in the optimization problem formulation by defining additional manufacturing constraints for individual shaft sections. Structural and dynamic performance of the finalized designs must be confirmed by additional theoretical and experimental analyses.

VI. Conclusions

The design optimization of twin-spool rotor systems is examined in the present study. The optimization environment developed in the previous works is extended to perform simultaneous sizing optimization of multiple shafts using the sequential quadratic programming technique with hybrid, analytical and numerical, sensitivity analysis. The inner radius and wall thickness of beam finite elements are selected as design variables. The optimization aim is to minimize the total mass of the shafts with constraints imposed on static stresses, natural frequencies, and unbalance response amplitudes.

The in-house beam-based finite-element method model with the Timoshenko beam formulation and two-node rigid disk elements used to perform static and rotordynamic analyses during the optimization is verified with a number of other, beam-based and 3-D axisymmetric, finite-element model implemented in the in-house code and in ANSYS Mechanical.

The developed optimization environment is successfully applied to the rotor system of a small-size turboprop engine that includes gas generator rotor, free-power turbine rotor, and the first stage of the gearbox. The presented results demonstrate good performance and efficiency of the developed optimization environment. The developed models and programs are capable of solving the problem of mass reduction for gas-turbine engine-rotor systems while keeping the rotordynamic characteristics within the specified ranges.

Based upon the findings presented in this paper, the following conclusions are drawn.

1) Lightweight structures of gas-turbine engines must be modeled with at least the Timoshenko beam elements and one-dimensional rigid disk elements or more sophisticated FE models. The first stage of the gearbox must be considered in the model to predict accurately the rotordynamic behavior of the considered free-power turbine rotor system.

2) Using the numerical sensitivity analysis for the modal equation positively affects the optimization process in terms of convergence and stability, but it increases the overall time of the optimization run.

3) The optimal designs A and B demonstrate the potential of mass reduction in the considered twin-spool rotor systems with all defined constraints being satisfied. The obtained total mass reduction is well above 60%. However, the optimal shaft shapes A and B are significantly different from the baseline design and would require substantial changes in the engine layout and redesigning other engine components.

4) The optimal design C obtained with additional constraints on design variables is a more practically valuable design that could be considered for the implementation in the existing prototype engine. The total mass of both shafts in the optimized configuration C is still less than 50% of the baseline design mass.

The developed optimization process provides preliminary designs with improved characteristics for further detailed analysis and

testing. The obtained total mass reduction in the presented results is well above 50% as compared to the baseline configuration taken from the prototype engine. However, the realizable mass reduction would be less pronounced when all other necessary technological requirements and results of advanced modeling and testing would be taken into account.

Appendix: Local Finite-Element Matrices for Timoshenko Beam and Disk Element

Figure A1 shows the schematic of the beam element.

Following are the local finite-element matrices for the Timoshenko beam and disk element:

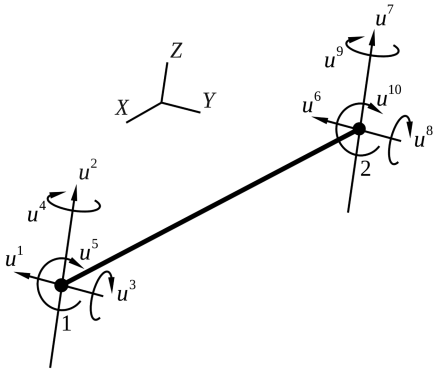

Fig. A1 Schematic of the Timoshenko beam element with 10 degrees of freedom.

$$\boldsymbol{k}^e = \frac{EI^a}{L^3(1+c_s)}\begin{bmatrix}
12 & & & & & & & & & \\
0 & 12 & & & & & & & & \\
0 & 6L & L^2(4+c_s) & & & & & & & \\
-6L & 0 & 0 & L^2(4+c_s) & & & & \text{Symmetric} & & \\
0 & 0 & 0 & 0 & K_t(1+c_s) & & & & & \\
-12 & 0 & 0 & 6L & 0 & 12 & & & & \\
0 & -12 & -6L & 0 & 0 & 0 & 12 & & & \\
0 & 6L & L^2(2-c_s) & 0 & 0 & 0 & -6L & L^2(4+c_s) & & \\
-6L & 0 & 0 & L^2(2-c_s) & 0 & 6L & 0 & 0 & L^2(4+c_s) & \\
0 & 0 & 0 & 0 & -K_t(1+c_s) & 0 & 0 & 0 & 0 & K_t(1+c_s)
\end{bmatrix} \tag{A1}$$

$$\boldsymbol{g}^e = \frac{\omega I^p}{30L}\begin{bmatrix}
0 & & & & & & & & & \\
-36 & 0 & & & & & & & & \\
3L & 0 & 0 & & & & & & & \\
0 & 3L & -4L^2 & 0 & & & & \text{Skew-symmetric} & & \\
0 & 0 & 0 & 0 & 0 & & & & & \\
0 & -36 & 3L & 0 & 0 & 0 & & & & \\
36 & 0 & 0 & 3L & 0 & -36 & 0 & & & \\
3L & 0 & 0 & -L^2 & 0 & -3L & 0 & 0 & & \\
0 & 3L & L^2 & 0 & 0 & 0 & -3L & -4L^2 & 0 & \\
0 & 0 & 0 & 0 & 0 & 0 & 0 & 0 & 0 & 0
\end{bmatrix} \tag{A2}$$

$$\boldsymbol{m}_t^e = \frac{\mu^m L}{420(1+c_s)^2}\begin{bmatrix}
156 & & & & & & & & & \\
0 & 156 & & & & & & & & \\
0 & 22L & 4L^2 & & & & & & & \\
-22L & 0 & 0 & 4L^2 & & & & \text{Symmetric} & & \\
0 & 0 & 0 & 0 & M_t(1+c_s)^2 & & & & & \\
54 & 0 & 0 & -13L & 0 & 156 & & & & \\
0 & 54 & 13L & 0 & 0 & 0 & 156 & & & \\
0 & -13L & -3L^2 & 0 & 0 & 0 & -22L & 4L^2 & & \\
13L & 0 & 0 & -3L^2 & 0 & 22L & 0 & 0 & 4L^2 & \\
0 & 0 & 0 & 0 & 0.5M_t(1+c_s)^2 & 0 & 0 & 0 & 0 & M_t(1+c_s)^2
\end{bmatrix} \tag{A3}$$

$$\boldsymbol{m}_{t,cs}^e = \frac{\mu^m L c_s}{120(1+c_s)^2}\begin{bmatrix}
84+40c_s & & & & & & & & & \\
0 & 84+40c_s & & & & & & & & \\
0 & -L(11+5c_s) & L^2(2+c_s) & & & & & & & \\
L(11+5c_s) & 0 & 0 & L^2(2+c_s) & & & & \text{Symmetric} & & \\
0 & 0 & 0 & 0 & 0 & & & & & \\
36+20c_s & 0 & 0 & -L(9+5c_s) & 0 & 84+40c_s & & & & \\
0 & 36+20c_s & L(9+5c_s) & 0 & 0 & 0 & 84+40c_s & & & \\
0 & -L(9+5c_s) & -L^2(2+c_s) & 0 & 0 & 0 & L(11+5c_s) & L^2(2+c_s) & & \\
L(9+5c_s) & 0 & 0 & -L^2(2+c_s) & 0 & -L(11+5c_s) & 0 & 0 & L^2(2+c_s) & \\
0 & 0 & 0 & 0 & 0 & 0 & 0 & 0 & 0 & 0
\end{bmatrix} \tag{A4}$$

$$\boldsymbol{m}_r^e = \frac{\rho I^a}{30L(1+c_s)^2}\begin{bmatrix} 36 & & & & & & & & & \\ 0 & 36 & & & & & & & & \\ 0 & 3L & 4L^2 & & & & & & & \\ -3L & 0 & 0 & 4L^2 & & & \text{Symmetric} & & & \\ 0 & 0 & 0 & 0 & 0 & & & & & \\ -36 & 0 & 0 & 3L & 0 & 36 & & & & \\ 0 & -36 & -3L & 0 & 0 & 0 & 36 & & & \\ 0 & 3L & -L^2 & 0 & 0 & 0 & -3L & 4L^2 & & \\ -3L & 0 & 0 & -L^2 & 0 & 3L^2 & 0 & 0 & 4L^2 & \\ 0 & 0 & 0 & 0 & 0 & 0 & 0 & 0 & 0 & 0 \end{bmatrix} \tag{A5}$$

$$\boldsymbol{m}_{r,cs}^e = \frac{\rho I^a c_s}{6L(1+c_s)^2}\begin{bmatrix} 0 & & & & & & & & & \\ 0 & 0 & & & & & & & & \\ 0 & -3L & L^2(1+2c_s) & & & & & & & \\ 3L & 0 & 0 & L^2(1+2c_s) & & & \text{Symmetric} & & & \\ 0 & 0 & 0 & 0 & 0 & & & & & \\ 0 & 0 & 0 & -3L & 0 & 0 & & & & \\ 0 & 0 & 3L & 0 & 0 & 0 & 0 & & & \\ 0 & -3L & -L^2(1-c_s) & 0 & 0 & 0 & 3L & L^2(1+2c_s) & & \\ 3L & 0 & 0 & -L^2(1-c_s) & 0 & -3L & 0 & 0 & L^2(1+2c_s) & \\ 0 & 0 & 0 & 0 & 0 & 0 & 0 & 0 & 0 & 0 \end{bmatrix} \tag{A6}$$

$$\boldsymbol{m}^e = \boldsymbol{m}_t^e + \boldsymbol{m}_{t,cs}^e + \boldsymbol{m}_r^e + \boldsymbol{m}_{r,cs}^e \tag{A7}$$

$$\boldsymbol{m}^d = \begin{bmatrix} m_d & 0 & 0 & 0 & 0 \\ 0 & m_d & 0 & 0 & 0 \\ 0 & 0 & I_d & 0 & 0 \\ 0 & 0 & 0 & I_d & 0 \\ 0 & 0 & 0 & 0 & 0 \end{bmatrix}; \qquad \boldsymbol{g}^d = \begin{bmatrix} 0 & 0 & 0 & 0 & 0 \\ 0 & 0 & 0 & 0 & 0 \\ 0 & 0 & 0 & J_d & 0 \\ 0 & 0 & -J_d & 0 & 0 \\ 0 & 0 & 0 & & 0 \end{bmatrix}; \qquad \boldsymbol{m}_{1D}^d = \boldsymbol{T}'\boldsymbol{m}^d\boldsymbol{T}; \qquad \boldsymbol{T} = \begin{bmatrix} 1 & 0 & 0 & -L_{1D}/2 & 0 \\ 0 & 1 & L_{1D}/2 & 0 & 0 \\ 0 & 0 & 1 & 0 & 0 \\ 0 & 0 & 0 & 1 & 0 \\ 0 & 0 & 0 & 0 & 1 \end{bmatrix} \tag{A8}$$

Acknowledgments

The presented work has been funded by the European Commission within the Seventh Framework Programme (FP7) project "Efficient Systems and Propulsion for Small Aircraft" (contract ACP1-GA-2011-284859-ESPOSA).

References

[1] Chiang, H.-W. D., Hsu, C.-N., and Tu, S.-H., "Rotor-Bearing Analysis for Turbomachinery Single- and Dual-Rotor Systems," *Journal of Propulsion and Power*, Vol. 20, No. 6, Nov. 2004, pp. 1096–1104. doi:10.2514/1.3133

[2] Jeon, S. M., Kwak, H. D., Yoon, S. H., and Kim, J., "Rotordynamic Analysis of a Turbopump with the Casing Structural Flexibility," *Journal of Propulsion and Power*, Vol. 24, No. 3, May 2008, pp. 433–436. doi:10.2514/1.33551

[3] Shiau, T., and Hwang, J., "Minimum Weight Design of a Rotor Bearing System with Multiple Frequency Constraints," *ASME Journal of Engineering for Gas Turbines and Power*, Vol. 110, No. 4, 1988, pp. 592–599. doi:10.1115/1.3240176

[4] Shiau, T., and Chang, J., "Multi-Objective Optimization of Rotor-Bearing System with Critical Speed Constraints," *ASME Journal of Engineering for Gas Turbines and Power*, Vol. 115, No. 2, 1993, pp. 246–255. doi:10.1115/1.2906701

[5] Chen, T.-Y., and Wang, B., "Optimum Design of Rotor-Bearing Systems with Eigenvalue Constraints," *ASME Journal of Engineering for Gas Turbines and Power*, Vol. 115, No. 2, 1993, pp. 256–260. doi:10.1115/1.2906702

[6] Lee, D.-S., and Choi, D.-H., "Reduced Weight Design of a Flexible Rotor with Ball Bearing Stiffness Characteristics Varying with Rotational Speed and Load," *ASME Journal of Vibration and Acoustics*, Vol. 122, No. 3, 2000, pp. 203–208. doi:10.1115/1.1303066

[7] Lin, Y.-H., and Lin, S.-C., "Optimal Weight Design of Rotor Systems with Oil-Film Bearings Subjected to Frequency Constraints," *Finite Elements in Analysis and Design*, Vol. 37, No. 10, 2001, pp. 777–798. doi:10.1016/S0168-874X(00)00072-X

[8] Strauß, F., Inagaki, M., and Starke, J., "Reduction of Vibration Level in Rotordynamics by Design Optimization," *Structural and Multidisci-*

plinary Optimization, Vol. 34, No. 2, 2007, pp. 139–149.
doi:10.1007/s00158-006-0065-3

[9] Rajan, M., Rajan, S., Nelson, H., and Chen, W., "Optimal Placement of Critical Speeds in Rotor-Bearing Systems," *ASME Journal of Vibration and Acoustics*, Vol. 109, No. 2, 1987, pp. 152–157.
doi:10.1115/1.3269407

[10] Huang, S.-C., and Lin, C.-A., "Sensitivity Analysis and Optimization of Undamped Rotor Critical Speeds to Supports Stiffness," *ASME Journal of Vibration and Acoustics*, Vol. 124, No. 2, 2002, pp. 296–301.
doi:10.1115/1.1456083

[11] Cole, M., Wongratanaphisan, T., and Keogh, P., "On LMI-Based Optimization of Vibration and Stability in Rotor System Design," *ASME Journal of Engineering for Gas Turbines and Power*, Vol. 128, No. 3, 2006, pp. 677–684.
doi:10.1115/1.2135818

[12] Shiau, T., Chang, J., and Lu, W., "Multilevel Optimization of the Geared Rotor-Bearing System for Multi-Objectives with Critical Speed Constraints," *ASME Turbo Expo 2004: Power for Land, Sea, and Air*, Vol. 6, American Soc. of Mechanical Engineers Paper :GT2004-54066, Fairfield, NJ, June 2004, pp. 755–762.
doi:10.1115/GT2004-54066

[13] Angantyr, A., and Aidanpää, J., "A Pareto-Based Genetic Algorithm Search Approach to Handle Damped Natural Frequency Constraints in Turbo Generator Rotor System Design," *ASME Journal of Engineering for Gas Turbines and Power*, Vol. 126, No. 3, 2004, pp. 619–625.
doi:10.1115/1.1760529

[14] Yang, B., Choi, S., and Kim, Y., "Vibration Reduction Optimum Design of a Steam-Turbine Rotor-Bearing System Using a Hybrid Genetic Algorithm," *Structural and Multidisciplinary Optimization*, Vol. 30, No. 1, 2005, pp. 43–53.
doi:10.1007/s00158-004-0513-x

[15] Shiau, T.-N., Kang, C.-H., and Liu, D.-S., "Interval Optimization of Rotor-Bearing Systems with Dynamic Behavior Constraints Using an Interval Genetic Algorithm," *Structural and Multidisciplinary Optimization*, Vol. 36, No. 6, 2008, pp. 623–631.
doi:10.1007/s00158-007-0199-y

[16] Pugachev, A., Sheremetyev, A., Tykhomirov, V., and Timchenko, I., "Gradient-Based Optimization of a Turboprop Rotor System with Constraints on Stresses and Natural Frequencies," *6th AIAA Multidisciplinary Design Optimization Specialist Conference*, AIAA Paper 2010-3006, April 2010.

[17] Pugachev, A., "Application of Gradient-Based Optimization Methods for a Rotor System with Static Stress, Natural Frequency, and Harmonic Response Constraints," *Structural and Multidisciplinary Optimization*, Vol. 47, No. 6, 2013, pp. 951–962.
doi:10.1007/s00158-012-0867-4

[18] Kramer, E., *Dynamics of Rotors and Foundations*, Springer–Verlag, Berlin, 1993.

[19] Tisseur, F., "Backward Error and Condition of Polynomial Eigenvalue Problems," *Linear Algebra and Its Applications*, Vol. 309, Nos. 1–3, 2000, pp. 339–361.
doi:10.1016/S0024-3795(99)00063-4

[20] Adams, M. L. J., *Rotating Machinery Vibration: From Analysis to Troubleshooting*, Marcel Dekker, New York, 2001.

[21] Pugachev, A., Sheremetyev, A., Tykhomirov, V., and Shpilenko, O., "Finite Element Modeling and Vibration Analysis of a Free Power Turbine Subjected to Non-Synchronous Excitation," *Proceedings of the 9th IFToMM International Conference on Rotor Dynamics*, Springer, New York, May 2015.

[22] "ANSYS Mechanical APDL Advanced Analysis Guide," Release 14.5, ANSYS, Canonsburg, PA, 2012.

[23] Fletcher, R., *Practical Methods of Optimization. Volume 2: Constrained Optimization*, Wiley, New York, 1981, pp. 138–144.

[24] Arora, J., *Introduction to Optimum Design*, Elsevier, New York, 2004, pp. 400–407.

[25] Haug, E., Choi, K., and Komkov, V., *Design Sensitivity Analysis of Structural Systems*, Academic Press, New York, 1986, pp. 25–67.

[26] Friswell, M. I., and Adhikari, S., "Derivatives of Complex Eigenvectors Using Nelson's Method," *AIAA Journal*, Vol. 38, No. 12, 2000, pp. 2355–2357.
doi:10.2514/2.907